NADPH oxidase 4 attenuates cerebral artery changes during the progression of Marfan syndrome

Yara Onetti[1], Thayna Meirelles[2], Ana P Dantas[3], Katrin Schröder[4], Elisabet Vila[1], Gustavo Egea[2,3], Francesc Jiménez-Altayó[1]

[1]Departament de Farmacologia, de Terapèutica i de Toxicologia, Institut de Neurociències, Facultat de Medicina, Universitat Autònoma de Barcelona, Bellaterra, Spain. [2]Departament de Biologia Cel·lular, Immunologia i Neurociències, Facultat de Medicina, Universitat de Barcelona, Barcelona, Spain. [3]Institut Clínic del Tòrax, Institut d'Investigacions Biomèdiques August Pi i Sunyer (IDIBAPS), Barcelona, Spain. [4]Institute for Cardiovascular Physiology, Goethe-University Frankfurt, Frankfurt, Germany.

Correspondence: Dr F Jiménez-Altayó, Departament de Farmacologia, de Terapèutica i de Toxicologia, Facultat de Medicina, Universitat Autònoma de Barcelona, 08193 Bellaterra (Cerdanyola del Vallès), Spain. E-mail: francesc.jimenez@uab.cat, Tel: (+34) 93 581 1952; Fax: (+34) 93 581 1953

Running title: Nox4 mitigates cerebral artery changes in Marfan syndrome

ABSTRACT

Marfan syndrome (MFS) is a connective tissue disorder that is often associated with fibrillin-1 (*Fbn1*) gene mutation and characterized by cardiovascular alterations, predominantly ascending aortic aneurysms. Although neurovascular complications are uncommon in MFS, the improvement in Marfan patients' life expectancy is revealing other secondary alterations, potentially including neurovascular disorders. However, little is known about small vessel pathophysiology in MFS. MFS is associated with hyperactivated transforming growth factor (TGF)-β signaling, which, among numerous other downstream effectors, induces the Nox4 isoform of NADPH oxidase, a strong enzymatic source of H_2O_2. We hypothesized that MFS induces middle cerebral artery (MCA) alterations, and that Nox4 contributes to them. MCA properties from 3-, 6- or 9-month-old Marfan (*Fbn1*$^{C1039G/+}$) mice were compared with those from age/sex-matched wild-type littermates. At 6 months, Marfan compared with wild-type mice developed higher MCA wall/lumen (wild-type: 0.081 ± 0.004; Marfan: 0.093 ± 0.002; 60 mmHg; $P < 0.05$), coupled with increased reactive oxygen species production, TGF-β and Nox4 expression. However, wall stiffness and myogenic autoregulation did not change. To investigate the influence of Nox4 on cerebrovascular properties, we generated Marfan mice with Nox4 deficiency (Nox4$^{-/-}$). Strikingly, Nox4 deletion in Marfan mice aggravated MCA wall thickening (cross-sectional area; Marfan: 6660 ± 363 μm^2; Marfan Nox4$^{-/-}$: 8795 ± 824 μm^2; 60 mmHg; $P < 0.05$), accompanied by decreased TGF-β expression, and increased collagen deposition and Nox1 expression. These findings provide the first evidence that Nox4 mitigates cerebral artery structural changes in a murine model of MFS.

Keywords: fibrillin-1; neurovascular disorders; structural alterations; transforming growth factor-β; Nox4

NEW & NOTEWORTHY

This is the first study to characterize the cerebral artery properties in an animal model of Marfan syndrome. Importantly, we reveal a role for Nox4 in attenuating brain vascular structural changes in Marfan syndrome, which may confer protection against the development of neurovascular disorders during Marfan syndrome progression.

INTRODUCTION

Marfan syndrome (MFS) is an autosomal dominant connective tissue disorder with multiple clinical manifestations, including cardiovascular alterations (5, 26). Mutations of the gene encoding fibrillin-1 (*Fbn1*) are the underlying cause (17). Fibrillin-1 is a scaffolding protein that is crucial for elastin deposition and the formation of elastic fibers and laminae (41). Aortic aneurysm leading to aortic dissection and rupture is the event that contributes to premature mortality (5). Neurovascular disorders are uncommon in Marfan patients. In a retrospective hospital-based study, in which patients affected with MFS were seen between 1989 and 1997 (49), no major association of MFS with neurovascular complications has been clearly reported. In addition, the relationship between cerebral artery aneurysms and MFS has been questioned (10, 48, 49). Therefore, the current evidence does not conclusively support a link between MFS and neurovascular disorders. Advances in pharmacological and mainly surgical therapies have resulted in longer life expectancy for Marfan patients (39). However, one consequence of this undoubted improvement could be that Marfan patients are increasingly exposed to other complications, such as those of a neurovascular type. To understand the pathophysiological basis of MFS alterations, a variety of murine experimental models have been developed. The most commonly used is mice heterozygous for the *Fbn1* allele encoding a missense mutation (*Fbn1*$^{C1039G/+}$), which is representative of the most common class of mutation observed in Marfan patients. Marfan mice show impairments in aortic functional and mechanical properties that could contribute to the risk of aortic aneurysm formation (7, 8, 9). However, very little is known about the pathophysiology of small vessels in MFS. To our knowledge, only mesenteric resistance artery properties have been thoroughly analyzed, with reports of Marfan-associated increases in wall stiffness and vasomotor dysfunction (45, 46).

Fibrillin-1 form microfibrils, which are a reservoir of transforming growth factor-β (TGF-β) and thus contribute to different aspects of Marfan-related vascular pathophysiology (12, 19, 33). It is well-known that overexpression of TGF-β1 in the brain of non-Marfan animals contributes to cerebrovascular dysfunction (47). On the other hand, vascular NADPH oxidase is a critical source of oxidative stress (20). In this respect, NADPH oxidase 4 (Nox4) is the only family member expressed in the vascular wall (20) whose expression is regulated by TGF-β (6, 13, 22, 38). Nox4 generates H_2O_2 as a reactive oxygen species (ROS), and previous studies have suggested that H_2O_2 regulates arterial structure and function (44). Therefore, we hypothesized that Nox4 could be a relevant downstream effector of TGF-β in the cerebral vasculature in MFS. This hypothesis is based on experimental evidence that shows augmented oxidative stress in aortic and mesenteric artery dysfunction in MFS (46, 50), greater oxidative stress and Nox4 expression in cerebral than in systemic arteries (32), and the relevance of Nox4 as a source of oxidative stress in ischemic stroke (40).

Although vascular alterations in systemic arteries have been previously identified in a mouse model of MFS (7, 8, 9, 45, 46, 50), cerebral artery properties have not been investigated. If cerebrovascular abnormalities were present, they might contribute to susceptibility to the development of neurovascular complications. We therefore examined middle cerebral artery (MCA) properties during MFS progression, and subsequently the putative role of Nox4 in the potential alterations that have been observed.

MATERIALS AND METHODS

Animals

Three-, six- and nine-month-old male and female mice were similarly distributed across wild-type (n = 26) and *Fbn1*$^{C1039G/+}$ (Marfan; n = 25) groups. Marfan mice began with

matrices from the Jackson Laboratory (Charles River, Lyon, France). Moreover, 6-month-old wild-type Nox4$^{-/-}$ (n = 7) and Marfan Nox4$^{-/-}$ (n = 5) mice were used. To establish the Marfan Nox4$^{-/-}$ mice colony, initially wild-type Nox4$^{-/-}$ female mice (42) were bred with *Fbn1*$^{C1039G/+}$ (Marfan Nox4$^{+/+}$) male mice. From the resulting Nox4 heterozygous generation (Nox4$^{+/-}$), Marfan male mice were crossed with wild-type female mice to obtain Marfan Nox4$^{-/-}$ male mice that were selected and successively bred with wild-type Nox4$^{-/-}$ female mice. All mice were housed according to institutional guidelines (constant room temperature at 22 °C, 12 h light/dark cycle, 60% humidity, and water ad libitum). All of the experiments were performed under the guidelines established by Spanish legislation (RD 1201/2005) and according to the *Guide for the Care and Use of Laboratory Animals,* published by the United States National Institutes of Health (NIH Publications 85-23, revised 1996). Experiments were approved by the *Ethics Committee* of the Universitat de Barcelona, and were carried out in compliance with European legislation.

Tissue preparation

MCA from the right and left hemisphere was dissected under a surgical microscope and kept in ice-cold Krebs-Henseleit solution (KHS, composition in mM: NaCl 112.0; KCl 4.7; $CaCl_2$ 2.5; KH_2PO_4 1.1; $MgSO_4$ 1.2; $NaHCO_3$ 25.0; and glucose 11.1) gassed with 95% O_2 and 5% CO_2. The proximal segment of the MCA was immediately used for pressure myography, and at the end of the assay it was handled for nuclei distribution microscopic fluorescence studies (36) and picrosirius red staining (16). Distal MCA segments were used for immunofluorescence (36) and evaluation of superoxide anion production (36). Branches of the MCA and the remaining cerebral arteries were processed for analysis of mRNA levels (36).

Pressure myography

Structural, mechanical and myogenic properties of the MCA were studied with a pressure myograph (Danish Myo Tech, model P100; J.P. Trading, Aarhus, Denmark), as described (16, 36). Briefly, vessels were placed on two glass microcannulas and carefully adjusted so that the vessel walls were parallel without stretching them. Intraluminal pressure was then raised to 140 mmHg, and the artery was unbuckled by adjusting the cannulas. Afterwards, the artery was left to equilibrate for 45 min at 40 mmHg in gassed KHS (37°C). Intraluminal pressure was reduced to 3 mmHg, and a pressure–diameter curve (3-120 mmHg) was obtained. Internal and external diameters (D_{iCa} and D_{eCa}) were measured for 3 min at each intraluminal pressure. The artery was left to equilibrate for 30 min at 40 mmHg in gassed, calcium-free KHS (37°C; 0 Ca^{2+}: omitting calcium and adding 10 mM EGTA; Sigma-Aldrich, St Louis, MO) and a second pressure-diameter curve (3-120 mmHg) was obtained in passive conditions. Structural, mechanical and myogenic parameters were analyzed as described (16).

Nuclei distribution by confocal microscopy

Pressured (40 mmHg)-fixed intact MCA was stained with Hoechst 33342 nuclear dye (10 µg/ml; Sigma-Aldrich) for 30 min (16, 36). Once washing had been completed, arteries were mounted on slides with a well that was made from silicon spacers, to avoid artery deformation. The slides were visualized with a Leica TCS SP2 (Heidelberg, Germany) confocal system. Stacks of serial optical slices (0.4 µm thick) were captured from the adventitia to the lumen of each artery. The different MCA layers stained with Hoechst 33342 were clearly distinguished with confocal microscopy, according to the shape and/or orientation of the cell nuclei (1). At least two stacks of images of several regions were captured in each arterial segment. MetaMorph Image

Analysis software (Molecular Devices, Sunnyvale, CA) was used for quantification, as reported (16).

Elastin determination

Total elastin content was studied in MCA cross-sections (14 μm thick) on the basis of the autofluorescent properties of elastin, as described (35). The fluorescence intensity value was used as an estimate of elastin concentration, following the assumption that the concentration of elastin has a linear relationship with fluorescence intensity (3). Preparations were viewed using a laser scanning confocal microscope (Leica TCS SP2). All the images were taken under identical conditions of zoom (×1), laser intensity, brightness, and contrast. Quantitative analysis of elastin autofluorescence was performed with MetaMorph Image Analysis software (Molecular Devices). The fluorescence signal per area was measured in at least two rings from each animal, and the results were expressed as arbitrary units.

The content of elastic fibers in the internal elastic lamina (IEL) was studied in intact pressure (40 mmHg)-fixed MCA using a Leica TCS SP5 confocal microscope. Stacks of serial optical sections (0.3 μm thick) were captured from each artery. At least, two stacks of images of several regions were captured in each arterial segment. All the images were taken under identical conditions of zoom (×5), laser intensity, brightness, and contrast. Quantitative analysis was performed with MetaMorph Image Analysis software (Molecular Devices), as described (24).

Collagen determination by picrosirius red staining

MCA sections (14 μm thick) were stained with picrosirius red to determine total collagen (16). Images were taken using a Leica Leitz DMRB microscope equipped with

a Leica DC500 camera, and analyzed with MetaMorph Image Analysis software (Molecular Devices). Total collagen content was calculated as a percentage of the stained area of each image obtained under visible light in at least two rings from each animal, and the results were expressed as arbitrary units.

Immunofluorescence

Frozen transverse sections (14 μm thick) of MCA were incubated (1 h) with a goat polyclonal antibody against matrix metalloproteinase (MMP)-9 (1:100; R&D Systems, Inc., Minneapolis, MN). After being washed, sections were incubated (45 min) with the secondary antibody (1:200), a donkey anti-goat IgG conjugated to Cyanine 3 (Jackson ImmunoResearch Laboratories, West Grove, PA) at 37°C. The specificity of the immunostaining was verified by omission of the primary antibody, which abolished the fluorescence signal. Quantitative analysis of fluorescence was performed with MetaMorph Image Analysis software (Molecular Devices) and the results were expressed as arbitrary units (36).

Measurement of superoxide anion formation

The oxidative fluorescent dye dihydroethidium (DHE) was used to evaluate production of superoxide anion *in situ* (14-μm thick sections) (18). Quantitative analysis of DHE-derived fluorescence was performed with MetaMorph Image Analysis software (Molecular Devices), as reported (16, 36).

Quantitative real-time PCR (qRT-PCR)

mRNA expression was quantified by Sybr green-based quantitative real time-PCR as described (34). The expression of mRNA for GAPDH of 18S ribosomal RNA was used as an internal control. qRT-PCR reactions were set up following the manufacturer's guidelines. Ct values obtained for each gene were referenced to GAPDH 18S (ΔΔCt) and converted to the linear form using the term $2^{-\Delta\Delta Ct}$ as a value directly proportional to the copy number of cDNA and the initial quantity of mRNA (34).

Statistics

Results are expressed as means ± SE of the number (*n*) of mice indicated in the legends for Figs. 1-6. The difference between wild-type or Marfan mice and the effect of Nox4 deletion was assessed by a two-way ANOVA with Tukey's post-test to compare groups. Data analysis was carried out using GraphPad Prism version 6 software. A value of $P < 0.05$ was considered significant.

RESULTS

Structural, mechanical and myogenic properties of MCA during MFS progression

To obtain MCA structural parameters, external and internal diameters were measured under fully relaxed conditions (0 Ca^{2+}-KHS). We did not find a significant difference in external (3 months; wild-type: 167.33 ± 3.41 μm, *n* = 9; Marfan: 169.86 ± 4.23 μm, *n* = 7; 6 months; wild-type: 171.00 ± 5.03 μm, *n* = 10; Marfan: 167.18 ± 3.79 μm, *n* = 11; 9 months; wild-type: 168.71 ± 6.09 μm, *n* = 7; Marfan: 163.14 ± 2.78 μm, *n* = 7; 60 mmHg) or internal (3 months; wild-type: 143.00 ± 2.46 μm, *n* = 9; Marfan: 145.00 ± 4.53 μm, *n* = 7; 6 months; wild-type: 146.60 ± 5.20 μm, *n* = 10; Marfan: 141.00 ± 3.25 μm, *n* = 11; 9 months; wild-type: 143.43 ± 6.36 μm, *n* = 7; Marfan: 136.00 ± 2.64 μm, *n* = 7; 60 mmHg) diameter in wild-type versus Marfan mice in any age group under study.

At 3 months, structural parameters were similar in vessels from control and Marfan mice. However, at 6 months of age, unlike cross-sectional area (Fig. 1*A*) and wall thickness (results not shown), the wall/lumen (Fig. 1*B*) was higher ($P < 0.05$) in Marfan than in wild-type mice, difference that disappeared at 9 months of age. Additionally, neither the cross-sectional area (Fig. 1*A*) nor the wall thickness (results not shown) was modified in Marfan mice at this age.

Wall stiffness is a mechanical parameter that can be determined from the stress-strain relationship (2). Since the stress-strain curve is not linear, it is more appropriate to obtain the slope of the curve (β-value). At all mice ages studied, the stress-strain relationship and the β-values were similar, which indicates that MCA stiffness is not altered in Marfan mice (Fig. 2*A*).

We did not find a significant difference in internal diameter in active conditions in wild-type versus Marfan mice in any age group under study (3 months; wild-type: 131.11 ± 3.41 μm, $n = 9$; Marfan: 135.14 ± 3.94 μm, $n = 7$; 6 months; wild-type: 121.00 ± 8.40 μm, $n = 9$; Marfan: 121.70 ± 3.93 μm, $n = 10$; 9 months; wild-type: 124.86 ± 5.11 μm, $n = 7$; Marfan: 116.57 ± 4.98 μm, $n = 7$; 60 mmHg). The analysis of myogenic response as a function of pressure obtained from internal diameter reductions in active relative to passive (0 Ca^{2+}-KHS) conditions revealed that arteries from 3-month-old wild-type mice had less ($P < 0.05$) myogenic tone than arteries of mice from 6 and 9 months (Fig. 2*B*). However, neither the analysis of myogenic response as a function of pressure (Fig. 2*B*) nor the slope of these curves (myogenic reactivity; Table 1) showed significant differences between wild-type and Marfan MCA in all age groups.

ROS production in cerebral arteries of Marfan mice and the impact of Nox4 deletion

We next measured expression levels of the most relevant NADPH oxidases of brain vasculature, as well as ROS production in cerebral arteries from wild-type and Marfan mice (Fig. 3). We evaluated mRNA levels of NADPH oxidase (a major source of vascular superoxide anion) catalytic (Nox1, Nox2, Nox4) and regulatory ($p22^{phox}$) subunits. Marfan cerebral arteries did not show differences in Nox1 and $p22^{phox}$ mRNA expression levels compared with wild-type mice (Fig. 3*A*). In contrast, mRNA levels of Nox4 were significantly higher ($P < 0.05$) in Marfan mice (Fig. 3*A*).

To understand the physiological meaning of increased Nox4 expression in MCA of Marfan mice, we generated a Marfan mice model, which was deleted for Nox4 ($Nox4^{-/-}$). Taking into account the aforementioned results, we chose animals at six months, in which the most significant vascular changes were observed. Absence of Nox4 expression *per se* did not alter either Nox1 or $p22^{phox}$ mRNA levels (Fig. 3*A*). However, Nox4 deficiency in Marfan mice led to higher ($P < 0.05$) Nox1 mRNA expression levels than in wild-type mice (Fig. 3*A*). Unfortunately, Nox2 mRNA levels were undetectable. We also analyzed mRNA levels of Poldip2, which binds to $p22^{phox}$ and enhances Nox4 activity (30), and no differences were observed (results not shown). ROS levels were evaluated by DHE-derived fluorescence, and they were higher along the MCA wall of Marfan (two-way ANOVA; $P < 0.01$) mice than in wild-type mice (Fig. 3*B*). However, post-test analysis showed significant increases ($P < 0.05$) in Marfan compared to wild-type mice, but not between Marfan $Nox4^{+/+}$ and Marfan $Nox4^{-/-}$. This suggests that the superoxide anion is not increased via Nox4, but probably through other Nox such as Nox1.

TGF-β production in cerebral arteries of Marfan mice and the impact of Nox4 deletion

We evaluated TGF-β expression in cerebral arteries from wild-type and Marfan mice in the presence and absence of Nox4. Quantitative analysis of TGF-β mRNA levels showed higher ($P < 0.05$) mRNA expression in Marfan than in wild-type mice (Fig. 4). However, Nox4 deletion attenuated ($P < 0.001$) TGF-β mRNA expression levels. These results suggest that increases in local TGF-β expression might contribute to augmenting Nox4 expression in the MCA of Marfan mice in a feed-forward fashion.

Structural, mechanical and myogenic properties of MCA after Nox4 deletion

We next studied the contribution of Nox4 to the MCA properties of wild-type and Marfan mice (Fig. 5). External (wild-type: 170.40 ± 5.36 μm, $n = 5$; Marfan: 169.33 ± 5.52 μm, $n = 6$; wild-type Nox4$^{-/-}$: 159.80 ± 4.64 μm, $n = 5$; Marfan Nox4$^{-/-}$: 178.00 ± 4.35 μm, $n = 5$; 60 mmHg) and internal (wild-type: 146.20 ± 4.74 μm, $n = 5$; Marfan: 142.17 ± 5.12 μm, $n = 6$; wild-type Nox4$^{-/-}$: 134.60 ± 5.14 μm, $n = 5$; Marfan Nox4$^{-/-}$: 142.80 ± 6.41 μm, $n = 5$; 60 mmHg) diameters under 0 Ca^{2+}-KHS did not differ in wild-type Nox4$^{-/-}$ compared with wild-type or Marfan mice. However, external diameters in MCA from Marfan Nox4$^{-/-}$ were more enlarged ($P < 0.01$) than in wild-type Nox4$^{-/-}$ mice. It is important to highlight that the absence of Nox4 expression *per se* did not alter the MCA structure. In contrast, deletion of Nox4 in Marfan mice led to an increase ($P < 0.05$) at high intraluminal pressures (from 60 to 120 mmHg) in cross-sectional area (Fig. 5*A*) and wall/lumen (Fig. 5*B*), but not wall thickness (results not shown). Nevertheless, Nox4 deficiency did not alter the wall stiffness (Fig. 5*C*), the internal diameter in active conditions (wild-type: 115.60 ± 9.93 μm, $n = 5$; Marfan: 113.83 ± 3.10 μm, $n = 6$; wild-type Nox4$^{-/-}$: 120.25 ± 3.90 μm, $n = 4$; Marfan Nox4$^{-/-}$: 119.20 ± 4.55 μm, $n = 5$; 60 mmHg), the myogenic response as a function of pressure (Fig. 5*D*), and the myogenic reactivity (wild-type: 0.133 ± 0.080, $n = 4$; Marfan: 0.077 ± 0.063, $n = 6$; wild-type Nox4$^{-/-}$: 0.033 ± 0.062, $n = 4$; Marfan Nox4$^{-/-}$: 0.007 ± 0.030, $n = 5$).

Distribution of nuclei through the MCA wall

We next examined whether the aforementioned structural differences could be attributed to changes in the cell density of the MCA wall. To this aim, we analyzed the nuclei distribution from intact and pressurized MCA. As reported in Table 2, total wall, adventitial and media MCA volumes, as well as smooth muscle and endothelial cell number, were almost the same in Marfan and wild-type mice. However, the absence of Nox4 in Marfan mice led to an augmented wall volume ($P < 0.01$) and a decrease ($P < 0.05$) in adventitial cell number. Taken together, these results suggest that the MCA structural alterations occurring in Marfan mice of 6 months of age would not implicate an increase in the number of wall cell nuclei, regardless of the presence or absence of Nox4.

Elastin and collagen contents in the MCA wall

Total elastin fluorescence in MCA cross sections was similar among groups (wild-type: 91.8 ± 17.7, $n = 6$; Marfan: 66.8 ± 9.9, $n = 5$; wild-type Nox4$^{-/-}$: 80.8 ± 15.5, $n = 5$; Marfan Nox4$^{-/-}$: 86.8 ± 4.8, $n = 4$). In addition, analysis of internal elastic lamina (IEL) thickness from intact pressurized MCA showed no differences among groups (Table 2). Although values of the average fluorescence intensity per pixel indicated a similar amount of elastin in wild-type and Marfan mice, a reduction ($P < 0.05$) in IEL fluorescence was observed between Marfan Nox4$^{-/-}$ and Marfan Nox4$^{+/+}$mice (Table 2).

To investigate whether the observed MCA wall hypertrophy in Marfan mice could be a consequence of excess collagen deposition, we measured the expression and content of collagen and proteins involved in extracellular matrix (ECM) degradation. Neither mRNA levels of collagen 1A1 (Fig. 6*A*) nor collagen deposition along the MCA wall

(Fig. 6*B*) was altered in Marfan compared with wild-type mice. However, a Marfan-associated increase ($P < 0.05$) in matrix metalloproteinase (MMP)-9 mRNA levels was observed (Fig. 6*A*). Nox4$^{-/-}$ mice showed an intrinsic increase ($P < 0.05$) of MMP-9 mRNA (Fig. 6*A*) that was accompanied by decreased ($P < 0.05$) collagen 1A1 mRNA levels (Fig. 6*A*), with unchanged collagen deposition (Fig. 6*B*). Importantly, Nox4 deficiency in Marfan mice led to augmented ($P < 0.05$) collagen deposition (Fig. 6*B*), despite diminished ($P < 0.01$) collagen 1A1 and augmented ($P < 0.01$) MMP-9 mRNA levels (Fig. 6*A*). Protein expression of MMP-9, assessed by immunofluorescence, was higher ($P < 0.05$) in Marfan than in wild-type mice, and was attenuated ($P < 0.05$) by Nox4 deletion (Fig. 6*C*). Overall, these results suggest that collagen degradation is augmented in the MCA of Marfan mice, and that even though transcriptional negative feedback modulation is initiated, net collagen deposition seem to contribute to MCA hypertrophy in Marfan Nox4$^{-/-}$ mice.

DISCUSSION

The aim of the present study was to characterize for the first time the cerebral artery properties of a mouse heterozygous for a mutation in *Fbn1* (*Fbn1*$^{C1039G/+}$), which manifests many clinical features of MFS. We observed that cerebral arteries from Marfan mice, along the progression of the disease (evaluated by the appearance of aortic aneurysm), developed slightly increased wall/lumen, accompanied by unaltered wall stiffness and myogenic autoregulation. At the same time, it is well-known that Marfan mice show hyperactivation of TGF-β signaling (19, 33), which in turn is known that upregulates the expression of Nox4 (6, 13, 22). Consistently, MCA from Marfan mice increased TGF-β and Nox4 mRNA levels. To investigate the potential influence of the Nox4 signaling pathway in cerebral artery properties, we generated Marfan mice with abrogated Nox4 expression. Strikingly, the loss of Nox4 in Marfan mice

aggravated structural alterations, which reveals a critical role for Nox4 in preventing cerebrovascular changes in MFS.

Large cerebral arteries, like the MCA, contribute substantially to cerebrovascular resistance (21). In this scenario, cerebrovascular adaptations permit brain circulation to maintain cerebral blood flow and meet metabolic demands, despite cardiovascular disturbances (21, 25). In our mouse model of MFS, MCA wall/lumen was increased at 6 months of age, which suggests age-related (i.e. not pre-existing) minor cerebral artery structural alterations in MFS. The increase in wall/lumen is a known adaptive process that contributes to maintaining cerebrovascular resistance and protecting downstream microcirculation from elevated arterial blood pressure, which can subsequently lead to vascular dysfunction (2). However, we did not observe significant wall/lumen differences in 9-month-old mice, most likely due to the slight age-dependent decline of this parameter in wild-type mice. Remarkably, Marfan animals did not display significant alterations in MCA wall stiffness during aging. In contrast, both aorta (8) and mesenteric arteries (46) from Marfan mice showed enhanced wall stiffness. In addition, the lack of changes in middle cerebral artery myogenic tone and reactivity suggest that myogenic autoregulatory mechanisms are preserved. Taken together, the different magnitude of changes observed during MFS progression in systemic (7, 8, 9, 45, 46, 50) compared to cerebral arteries suggests region-specific differences in sensitivity to MFS, and highlights that cerebral blood flow is tightly regulated.

Increased ROS production and/or oxidative stress have been found to be involved in systemic artery alterations related to MFS (46, 50). Accordingly, we observe that, MCA from Marfan mice also showed augmented ROS generation when compared to wild-type. Even though ROS production is often linked to an increase in vascular collagen deposition (4), we did not detect significant collagen accumulation in MCA from 6-month-old Marfan mice. ECM breakdown mediated by MMP has been associated with thoracic aortic aneurysm in MFS (8). Here, we have found augmented MMP-9 protein

401 expression in the MCA of Marfan mice, which could explain the increase in collagen
402 degradation. In addition, although fibrillin-1 is a scaffolding protein that is crucial for
403 elastin assembly (41), fibrillin-1 defects in Marfan animals do not seem to be coupled
404 with an apparent disruption of MCA wall elastin. Collectively, the absence of major
405 Marfan-induced ECM alterations in MCA are in contrast with changes reported in aorta
406 (8, 12, 14), but support previous findings that challenge the supposed association
407 between MFS and cerebral artery aneurysms (10, 48, 49). Nevertheless, we have to be
408 cautious in generalizing these results to human beings, as our study is limited to one of
409 the various available experimental murine models of MFS, whose clinical symptoms
410 are highly variable depending on their penetrance.

411 Unlike wild-type mice, Marfan $Nox4^{-/-}$ compared with Marfan $Nox4^{+/+}$ mice presented
412 greater MCA collagen deposition, which is a sign of fibrosis and vascular damage,
413 despite showing a transcriptional negative feedback loop involving decreased collagen
414 1A1 and increased MMP-9. Augmentation of collagen deposition probably contributes
415 to increased MCA cross-sectional area in Marfan $Nox4^{-/-}$ mice, which was not
416 associated with alterations in wall stiffness. These data support previous findings that
417 changes in the quantity, distribution and organization of new collagen are determinant
418 to defining the stiffness of the arterial wall (4).

419 Recent studies report an inverse relationship between vascular H_2O_2 production and
420 collagen deposition (31, 44, 51). Nox4 is an important source of oxidative stress in
421 cerebral arteries (32) that seems to play a pathophysiological role in the brain (40).
422 However, unlike Nox1 and Nox2, Nox4 also exerts a protective role in the vasculature
423 (20, 27, 42). This difference could be due to Nox4 capacity to produce H_2O_2, which is
424 the main detectable ROS that is produced, rather than the superoxide anion (43). It has
425 been suggested that Poldip2-mediated, and possibly, Nox4-derived H_2O_2 production
426 could reduce aortic collagen deposition (30, 44). Consistent with this idea, studies
427 show convincing evidence that MMP-9 activation and expression is positively

428 modulated by H_2O_2 predisposing to aortic aneurysm formation (37). In our study, the
429 presence of Nox4 was associated with increased MMP-9 protein expression in the
430 MCA of Marfan mice. Besides, significant collagen deposition was only observed after
431 Nox4 deletion in Marfan mice. However, based on present data we cannot confirm
432 whether Nox4-derived H_2O_2 might repress MCA collagen deposition in MFS. In
433 addition, upregulation of aortic Nox1 can promote superoxide anion production and
434 collagen formation (15). Thus, we cannot exclude the possibility that a Nox4-dependent
435 negative modulatory effect on Nox1-derived superoxide anion production might also
436 contribute to mitigating collagen accumulation in the MCA of Marfan mice.

437 Current evidence has not established a clear link between MFS and neurovascular
438 disorders (10, 48, 49), but since life expectancy increases in MFS patients who have
439 been diagnosed and treated, they could be exposed to more potential causes of
440 neurovascular disorders. The present study is the first to report the development of
441 modest but potentially relevant cerebrovascular alterations in an experimental murine
442 model of MFS. This study also contributes to our understanding of the role of the TGF-
443 β/Nox4 signaling pathway in cerebral vasculature in healthy, and particularly in Marfan
444 patients, since we show that genetic deletion of Nox4 in Marfan mice induces collagen
445 deposition which contributes to arterial wall hypertrophy, thereby causing overt MCA
446 structural alterations. In fact, previous evidence suggests a pathophysiological role of
447 Nox4 in brain damage (40). Overall, the results of the present study suggest that Nox4
448 has a role in regulating cerebrovascular resistance in Marfan animals. Thus, our
449 findings lead to the hypothesis that an overall reduction in TGF-β signaling, an ongoing
450 therapeutic approach against aortic aneurysm formation in MFS (29), might have a
451 negative impact on brain circulation. Similarly, recent evidence supports a critical role
452 of TGF-β signaling in maintaining postnatal aortic homeostasis (23, 28), and an early
453 protective role of TGF-β during aortic aneurysm progression (11). However, further

evidence is required to corroborate that Nox4 activation could actually play a beneficial role in the cerebral circulation of Marfan patients.

ACKNOWLEDGMENTS

We are grateful to Federica Dinolfo and Vanessa Hernandez for their excellent technical assistance, to Dr. Darya Gorbenko Del Blanco for helpful comments, and to the confocal microscopy core from the Universitat Autònoma de Barcelona.

GRANTS

The research was funded by Ministerio de Ciencia e Innovación (SAF2010-19282; SAF2014-56111-R) grants to E.V., a Generalitat de Catalunya (2014SGR574) grant to E.V. and F.J-A., and grants from the Ministerio de Ciencia e Innovación (BFU23012-33932), the Fundación Ramon Areces (Areces11-07) and the Generalitat de Catalunya (2014SGR334) to G.E. G.E. also acknowledges the National Marfan Foundation for its support. Additionally, this work was supported by a Deutsche Forschungsgemeinschaft (DFG; SFB815/TP1) grant to K.S. Y.O. is a predoctoral fellow (FPU) of the Ministerio de Educación y Ciencia (Spain) and T.M. was supported by a fellowship from the National Council of Technological and Scientific Development - Science without Borders scholarship program (Brazilian Federal Government)

DISCLOSURES

No conflicts of interest, financial or otherwise, are declared by the author(s).

REFERENCES

1. Arribas SM, Hillier C, González C, McGrory S, Dominiczak AF, McGrath JC. Cellular aspects of vascular remodeling in hypertension revealed by confocal microscopy. *Hypertension* 30: 1455-1464, 1997.

2. Baumbach GL, Heistad DD. Remodeling of cerebral arterioles in chronic hypertension. *Hypertension* 13: 968-972, 1989.

3. Blomfield J, Farrar JF. The fluorescent properties of maturing arterial elastin. *Cardiovasc Res* 3: 161-170, 1969.

4. Briones AM, Arribas SM, Salaices M. Role of extracellular matrix in vascular remodeling of hypertension. *Curr Opin Nephrol Hypertens* 19: 187-194, 2010.

5. Canadas V, Vilacosta I, Bruna I, Fuster V. Marfan syndrome. Part 1: pathophysiology and diagnosis. *Nat Rev Cardiol* 7: 256-265, 2010.

6. Carmona-Cuenca I, Roncero C, Sancho P, Caja L, Fausto N, Fernández M, Fabregat I. Upregulation of the NADPH oxidase NOX4 by TGF-beta in hepatocytes is required for its pro-apoptotic activity. *J Hepatol* 49: 965-976, 2008.

7. Chung AW, Au Yeung K, Cortes SF, Sandor GG, Judge DP, Dietz HC, van Breemen C. Endothelial dysfunction and compromised eNOS/Akt signaling in the thoracic aorta during the progression of Marfan syndrome. *Br J Pharmacol* 150: 1075-1083, 2007a.

8. Chung AW, Au Yeung K, Sandor GG, Judge DP, Dietz HC, van Breemen C. Loss of elastic fiber integrity and reduction of vascular smooth muscle contraction resulting from the upregulated activities of matrix metalloproteinase-

2 and -9 in the thoracic aortic aneurysm in Marfan syndrome. *Circ Res* 101: 512-522, 2007b.

9. Chung AW, Yang HH, van Breemen C. Imbalanced synthesis of cyclooxygenase-derived thromboxane A2 and prostacyclin compromises vasomotor function of the thoracic aorta in Marfan syndrome. *Br J Pharmacol* 152: 305-312, 2007c.

10. Conway JE, Hutchins GM, Tamargo RJ. Marfan syndrome is not asso- ciated with intracranial aneurysms. *Stroke* 30:1632-1636, 1999.

11. Cook JR, Clayton NP, Carta L, Galatioto J, Chiu E, Smaldone S, Nelson CA, Cheng SH, Wentworth BM, Ramirez F. Dimorphic effects of transforming growth factor-β signaling during aortic aneurysm progression in mice suggest a combinatorial therapy for Marfan syndrome. *Arterioscler Thromb Vasc Biol* 35: 911-917, 2015.

12. Crosas-Molist E, Meirelles T, López-Luque J, Serra-Peinado C, Selva J, Caja L, Del Blanco DG, Uriarte JJ, Bertran E, Mendizábal Y, Hernández V, García-Calero C, Busnadiego O, Condom E, Toral D, Castellà M, Forteza A, Navajas D, Sarri E, Rodríguez-Pascual F, Dietz HD, Fabregat I, Egea G. Vascular Smooth Muscle Cell Phenotypic Changes in Patients With Marfan Syndrome. *Arterioscler Thromb Vasc Biol* 35: 960-972, 2015.

13. Cucoranu I, Clempus R, Dikalova A, Phelan PJ, Ariyan S, Dikalov S, Sorescu D. NADPH oxidase 4 mediates transforming growth factor-beta1-induced differentiation of cardiac fibroblasts into myofibroblasts. *Circ Res* 97: 900-907, 2005.

14. Cui JZ, Tehrani AY, Jett KA, Bernatchez P, van Breemen C, Esfandiarei M. Quantification of aortic and cutaneous elastin and collagen morphology in Marfan syndrome by multiphoton microscopy. *J Struct Biol* 187: 242-253, 2014.

15. Dammanahalli JK, Wang X, Sun Z. Genetic interleukin-10 deficiency causes vascular remodeling via the upregulation of Nox1. *J Hypertens* 29: 2116-2125, 2011.

16. Dantas AP, Onetti Y, Oliveira MA, Carvalho MH, Heras M, Vila E, Jiménez-Altayó F. Western diet consumption promotes vascular remodeling in non-senescent mice consistent with accelerated senescence, but does not modify vascular morphology in senescent ones. *Exp Gerontol* 55: 1-11, 2014.

17. Dietz HC, Cutting CR, Pyeritz RE, Maslen CL, Sakai LY, Corson GM, Puffenberger EG, Hamosh A, Nanthakumar EJ, Curristin SM, Stetten G, Meyers DA, Francomano CA. Marfan syndrome caused by a recurrent de novo missense mutation in the fibrillin gene. *Nature* 352: 337-339, 1991.

18. Dikalov S, Griendling KK, Harrison DG. Measurement of reactive oxygen species in cardiovascular studies. *Hypertension* 49: 717-727, 2007.

19. Doyle JJ, Gerber EE, Dietz HC. Matrix-dependent perturbation of TGFβ signaling and disease. *FEBS Lett* 586: 2003-2015, 2012.

20. Drummond GR, Sobey CG. Endothelial NADPH oxidases: which NOX to target in vascular disease? *Trends Endocrinol Metab* 25:452-463, 2014.

21. Faraci FM, Heistad DD. Regulation of large cerebral arteries and cerebral microvascular pressure. *Circ Res* 66: 8-17, 1990.

22. Hecker L, Vittal R, Jones T, Jagirdar R, Luckhardt TR, Horowitz JC, Pennathur S, Martinez FJ, Thannickal VJ. NADPH oxidase-4 mediates myofibroblast

activation and fibrogenic responses to lung injury. *Nat Med* 15: 1077-1081, 2009.

23. Hu JH, Wei H, Jaffe M, Airhart N, Du L, Angelov SN, Yan J, Allen JK, Kang I, Wight TN, Fox K, Smith A, Enstrom R, Dichek DA. Postnatal Deletion of the Type II Transforming Growth Factor-β Receptor in Smooth Muscle Cells Causes Severe Aortopathy in Mice. *Arterioscler Thromb Vasc Biol* 35: 2647-2656, 2015.

24. Jiménez-Altayó F, Martín A, Rojas S, Justicia C, Briones AM, Giraldo J, Planas AM, Vila E. Transient middle cerebral artery occlusion causes different structural, mechanical, and myogenic alterations in normotensive and hypertensive rats. *Am J Physiol Heart Circ Physiol* 293: H628-H635, 2007.

25. Johnson AC, Cipolla MJ. The cerebral circulation during pregnancy: adapting to preserve normalcy. *Physiology (Bethesda)* 30: 139-147, 2015.

26. Judge DP, Dietz HC. Marfan's syndrome. *Lancet* 366: 1965-1976, 2005.

27. Konior A, Schramm A, Czesnikiewicz-Guzik M, Guzik TJ. NADPH oxidases in vascular pathology. *Antioxid Redox Signal* 20: 2794-2814, 2014.

28. Li W, Li Q, Jiao Y, Qin L, Ali R, Zhou J, Ferruzzi J, Kim RW, Geirsson A, Dietz HC, Offermanns S, Humphrey JD, Tellides G. Tgfbr2 disruption in postnatal smooth muscle impairs aortic wall homeostasis. *J Clin Invest* 124: 755-767, 2014.

29. Loeys BL. Angiotensin receptor blockers: a panacea for Marfan syndrome and related disorders? Drug Discov Today. 20: 262-266, 2015.

30. Lyle AN, Deshpande NN, Taniyama Y, Seidel-Rogol B, Pounkova L, Du P, Papaharalambus C, Lassègue B, Griendling KK. Poldip2, a novel regulator of

571 Nox4 and cytoskeletal integrity in vascular smooth muscle cells. *Circ Res* 105:
572 249-259, 2009.

573 31. Maiellaro-Rafferty K, Weiss D, Joseph G, Wan W, Gleason RL, Taylor WR.
574 Catalase overexpression in aortic smooth muscle prevents pathological
575 mechanical changes underlying abdominal aortic aneurysm formation. *Am J*
576 *Physiol Heart Circ Physiol* 301: H355-H362, 2011.

577 32. Miller AA, Drummond GR, Schmidt HH, Sobey CG. NADPH oxidase activity and
578 function are profoundly greater in cerebral versus systemic arteries. *Circ Res*
579 97: 1055-1062, 2005.

580 33. Neptune ER, Frischmeyer PA, Arking DE, Myers L, Bunton TE, Gayraud B,
581 Ramirez F, Sakai LY, Dietz HC. Dysregulation of TGF-beta activation
582 contributes to pathogenesis in Marfan syndrome. *Nat Genet* 33: 407-411, 2003.

583 34. Novensa L, Selent J, Pastor M, Sandberg K, Heras M, Dantas AP. Equine
584 estrogens impair nitric oxide production and endothelial nitric oxide synthase
585 transcription in human endothelial cells compared with the natural 17{beta}-
586 estradiol. *Hypertension* 56: 405-411, 2010.

587 35. Ogalla E, Claro C, Alvarez de Sotomayor M, Herrera MD, Rodriguez-Rodriguez
588 R. Structural, mechanical and myogenic properties of small mesenteric arteries
589 from ApoE KO mice: characterization and effects of virgin olive oil diets.
590 *Atherosclerosis* 238: 55-63, 2015.

591 36. Onetti Y, Dantas AP, Pérez B, Cugota R, Chamorro A, Planas AM, Vila E,
592 Jiménez-Altayó F. Middle cerebral artery remodeling following transient brain
593 ischemia is linked to early postischemic hyperemia: a target of uric acid
594 treatment. *Am J Physiol Heart Circ Physiol* 308: H862-H874, 2015.

595 37. Parastatidis I, Weiss D, Joseph G, Taylor WR. Overexpression of catalase in
596 vascular smooth muscle cells prevents the formation of abdominal aortic
597 aneurysms. *Arterioscler Thromb Vasc Biol* 33: 2389-2396, 2013.

598 38. Peshavariya HM, Chan EC, Liu GS, Jiang F, Dusting GJ. Transforming growth
599 factor-β1 requires NADPH oxidase 4 for angiogenesis in vitro and in vivo. *J Cell*
600 *Mol Med* 18: 1172-1183, 2014.

601 39. Pyeritz RE, Loeys B. The 8th international research symposium on the Marfan
602 syndrome and related conditions. *Am J Med Genet A* 158: 42-49, 2012.

603 40. Radermacher KA, Wingler K, Langhauser F, Altenhöfer S, Kleikers P, Hermans
604 JJ, Hrabě de Angelis M, Kleinschnitz C, Schmidt HH. Neuroprotection after
605 stroke by targeting NOX4 as a source of oxidative stress. *Antioxid Redox Signal*
606 18: 1418-1427, 2013.

607 41. Reinhardt DP, Chalberg SC, Sakai LY. The structure and function of fibrillin.
608 *Ciba Found Symp* 192: 128-143, 1995.

609 42. Schroder K, Zhang M, Benkhoff S, Mieth A, Pliquett R, Kosowski J, Kruse C,
610 Luedike P, Michaelis UR, Weissmann N, Dimmeler S, Shah AM, and Brandes
611 RP. Nox4 is a protective reactive oxygen species generating vascular NADPH
612 oxidase. *Circ Res* 110: 1217-1225, 2012.

613 43. Serrander L, Cartier L, Bedard K, Banfi B, Lardy B, Plastre O, Sienkiewicz A,
614 Fórró L, Schlegel W, Krause KH. NOX4 activity is determined by mRNA levels
615 and reveals a unique pattern of ROS generation. *Biochem J* 406: 105-114,
616 2007.

617 44. Sutliff RL, Hilenski LL, Amanso AM, Parastatidis I, Dikalova AE, Hansen L,
618 Datla SR, Long JS, El-Ali AM, Joseph G, Gleason RL Jr, Taylor WR, Hart CM,
619 Griendling KK, Lassègue B. Polymerase delta interacting protein 2 sustains

vascular structure and function. *Arterioscler Thromb Vasc Biol* 33: 2154-2161, 2013.

45. Syyong HT, Chung AW, van Breemen C. Marfan syndrome decreases Ca2+ wave frequency and vasoconstriction in murine mesenteric resistance arteries without changing underlying mechanisms. *J Vasc Res* 48: 150-162, 2011.

46. Syyong HT, Chung AW, Yang HH, van Breemen C. Dysfunction of endothelial and smooth muscle cells in small arteries of a mouse model of Marfan syndrome. *Br J Pharmacol* 158: 1597-1608, 2009.

47. Tong XK, Nicolakakis N, Kocharyan A, Hamel E. Vascular remodeling versus amyloid beta-induced oxidative stress in the cerebrovascular dysfunctions associated with Alzheimer's disease. *J Neurosci* 25: 11165-11174, 2005.

48. van den Berg JS, Limburg M, Hennekam RC. Is Marfan syndrome associated with symptomatic intracranial aneurysms? *Stroke* 27:10-12, 1996.

49. Wityk RJ, Zanferrari C, Oppenheimer S. Neurovascular complications of marfan syndrome: a retrospective, hospital-based study. *Stroke* 33: 680-684, 2002.

50. Yang HH, van Breemen C, Chung AW. Vasomotor dysfunction in the thoracic aorta of Marfan syndrome is associated with accumulation of oxidative stress. *Vascul Pharmacol* 52: 37-45, 2010.

51. Zhou RH, Vendrov AE, Tchivilev I, Niu XL, Molnar KC, Rojas M, Carter JD, Tong H, Stouffer GA, Madamanchi NR, Runge MS. Mitochondrial oxidative stress in aortic stiffening with age: the role of smooth muscle cell function. *Arterioscler Thromb Vasc Biol* 32: 745-755, 2012.

FIGURE CAPTIONS

Fig. 1. Structural properties of middle cerebral arteries in 3-, 6- and 9-month-old wild-type and Marfan mice. (A) Cross-sectional area (CSA)-intraluminal pressure in passive conditions (0 Ca^{2+}-KHS) and (B) wall/lumen-intraluminal pressure. Results are the means ± SE from wild-type (3 months: *n* = 9; 6 months: *n* = 9; 9 months: *n* = 7) and Marfan (3 months: *n* = 7; 6 months: *n* = 11; 9 months: *n* = 7) mice. **P* < 0.05 by two-way ANOVA.

Fig. 2. Mechanical and myogenic properties of middle cerebral arteries in 3-, 6-, 9-month-old wild-type and Marfan mice. (A) Stress-Strain (D_i/D_o). (B) Internal diameter in active (2.5 mM Ca^{2+}-KHS; D_{iCa}) relative to passive (D_{i0Ca}) conditions. D_o, internal diameter at 3 mmHg; D_i, observed internal diameter from a given intravascular pressure. Results are the means ± SE from wild-type (3 months: *n* = 9; 6 months: *n* = 7-8; 9 months: *n* = 7) and Marfan (3 months: *n* = 7; 6 months: *n* = 7-11; 9 months: *n* = 6-7) mice.

Fig. 3. Influence of Nox4 deletion ($Nox4^{-/-}$) on reactive oxygen species production of middle cerebral arteries in 6-month-old wild-type and Marfan mice. (A) Comparative analysis of cerebral artery mRNA levels of the NADPH oxidase subunit Nox1, Nox4 and $p22^{phox}$. mRNA levels are expressed as $2^{-\Delta\Delta Ct}$ using 18S as internal control. (B) Representative photomicrographs and quantitative analysis of fluorescence intensity of confocal microscopic middle cerebral artery sections labelled with the oxidative dye dihydroethidium (DHE), which produces a red fluorescence when oxidized by superoxide anion. END, endothelium; SM, smooth muscle; ADV, adventitia. Results are the means ± SE from wild-type (*n* = 5), Marfan (*n* = 5), wild-type $Nox4^{-/-}$ (*n* = 5-7) and Marfan $Nox4^{-/-}$ (*n* = 5) mice. **P* < 0.05, ***P* < 0.01, ****P* < 0.001 by two-way ANOVA with Tukey's post-test. All experimental groups were compared against each other but only significant comparisons are indicated.

Fig. 4. Influence of Nox4 deletion ($Nox4^{-/-}$) on transforming growth factor (TGF)-β mRNA levels of cerebral arteries in 6-month-old wild-type and Marfan mice. mRNA levels are expressed as $2^{-\Delta\Delta Ct}$ using 18S as internal control. Results are the means ± SE from wild-type (*n* = 5), Marfan (*n* = 5), wild-type $Nox4^{-/-}$ (*n* = 7) and Marfan $Nox4^{-/-}$ (*n* = 5) mice. **P* < 0.05, ****P* < 0.001 by two-way ANOVA with Tukey's post-test. All experimental groups were compared against each other but only significant comparisons are indicated.

Fig. 5. Influence of Nox4 deletion ($Nox4^{-/-}$) on structural, mechanical and myogenic properties of middle cerebral arteries in 6-month-old wild-type and Marfan mice. (A) Cross-sectional area (CSA)-intraluminal pressure in passive conditions (0 Ca^{2+}-KHS). (B) wall/lumen-intraluminal pressure. (C) Stress-Strain (D_i/D_o). (D) Internal diameter in active (2.5 mM Ca^{2+}-KHS; D_{iCa}) relative to passive (D_{i0Ca}) conditions. D_o, internal diameter at 3 mmHg; D_i, observed internal diameter from a given intravascular pressure. Results are the means ± SE from wild-type (*n* = 5), Marfan (*n* = 6), wild-type $Nox4^{-/-}$ (*n* = 5) and Marfan $Nox4^{-/-}$ (*n* = 5) mice. **P* < 0.05 by two-way ANOVA. All experimental groups were compared against each other but only significant comparisons are indicated.

Fig. 6. Influence of Nox4 deletion ($Nox4^{-/-}$) on collagen expression and homeostasis of middle cerebral arteries in 6-month-old wild-type and Marfan mice. (A) Comparative analysis of cerebral artery mRNA levels of collagen 1A1 (Col1A1) and matrix metalloproteinase (MMP)-9. mRNA levels are expressed as $2^{-\Delta\Delta Ct}$ using 18S as internal control. (B) Representative photomicrographs and quantitative analysis of total middle cerebral artery collagen staining using picrosirius red. (C) Representative photomicrographs and quantification of MMP-9 immunofluorescence of confocal microscopic middle cerebral artery sections. Results are the means ± SE from wild-type (*n* = 5-7), Marfan (*n* = 5), wild-type $Nox4^{-/-}$ (*n* = 4-5) and Marfan $Nox4^{-/-}$ (*n* = 5) mice. **P* < 0.05; ***P* < 0.01 by two-way ANOVA with Tukey's post-test. All experimental

groups were compared against each other but only significant comparisons are indicated.

Table 1 Slope value (myogenic reactivity) of the myogenic response as a function of pressure curve in middle cerebral arteries from 3-, 6- and 9-month-old wild-type and Marfan mice.

	wild-type	**Marfan**
Age (months)		
3	0.062 ± 0.033	0.043 ± 0.033
6	0.095 ± 0.038	0.108 ± 0.061
9	0.104 ± 0.049	0.064 ± 0.027

Results are the means ± SE from wild-type (3 months: *n* = 9; 6 months: *n* = 7; 9 months: *n* = 7) and Marfan (3 months: *n* = 7; 6 months: *n* = 7; 9 months: *n* = 7) mice.

Table 2 Comparison of nuclei distribution and internal elastic lamina elastin content in pressurized segments of middle cerebral arteries from 6-month-old wild-type and Marfan mice in the presence and absence of Nox4.

	$Nox4^{+/+}$		**$Nox4^{-/-}$**	
	wild-type	**Marfan**	**wild-type**	**Marfan**
Wall volume (mm^3)	0.006 ± 0.0004	0.007 ± 0.0002	0.006 ± 0.0002	0.008 ± 0.0008**
Adventitial volume (mm^3)	0.004 ± 0.0004	0.004 ± 0.0008	0.004 ± 0.0005	0.004 ± 0.0015
Media volume (mm^3)	0.002 ± 0.0007	0.002 ± 0.0006	0.002 ± 0.0006	0.002 ± 0.0007
Number of AC/mm^3	144 ± 105	399 ± 96	158 ± 102	34 ± 21*
Number of SMC/mm^3	1279 ± 129	1131 ± 118	1115 ± 177	1302 ± 232
Total number of EC	781 ± 71	553 ± 133	745 ± 138	897 ± 66
IEL thickness (μm)	2.9 ± 0.4	3.0 ± 0.4	3.4 ± 0.6	2.6 ± 0.2
IEL fluorescence intensity (average pixel)	23.6 ± 6.5	28.6 ± 3.8	22.3 ± 3.5	13.5 ± 2.0*

AC, adventitial cells; SMC, smooth muscle cells; EC, endothelial cells; IEL, internal elastic lamina. Results are the means ± SE from wild-type (n = 5), Marfan (n = 5), wild-type $Nox4^{-/-}$ (n = 5) and Marfan $Nox4^{-/-}$ (n = 5) mice. * $P < 0.05$, ** $P < 0.01$, Marfan vs. Marfan $Nox4^{-/-}$ by two-way ANOVA with Tukey's post-test.

Fig. 1

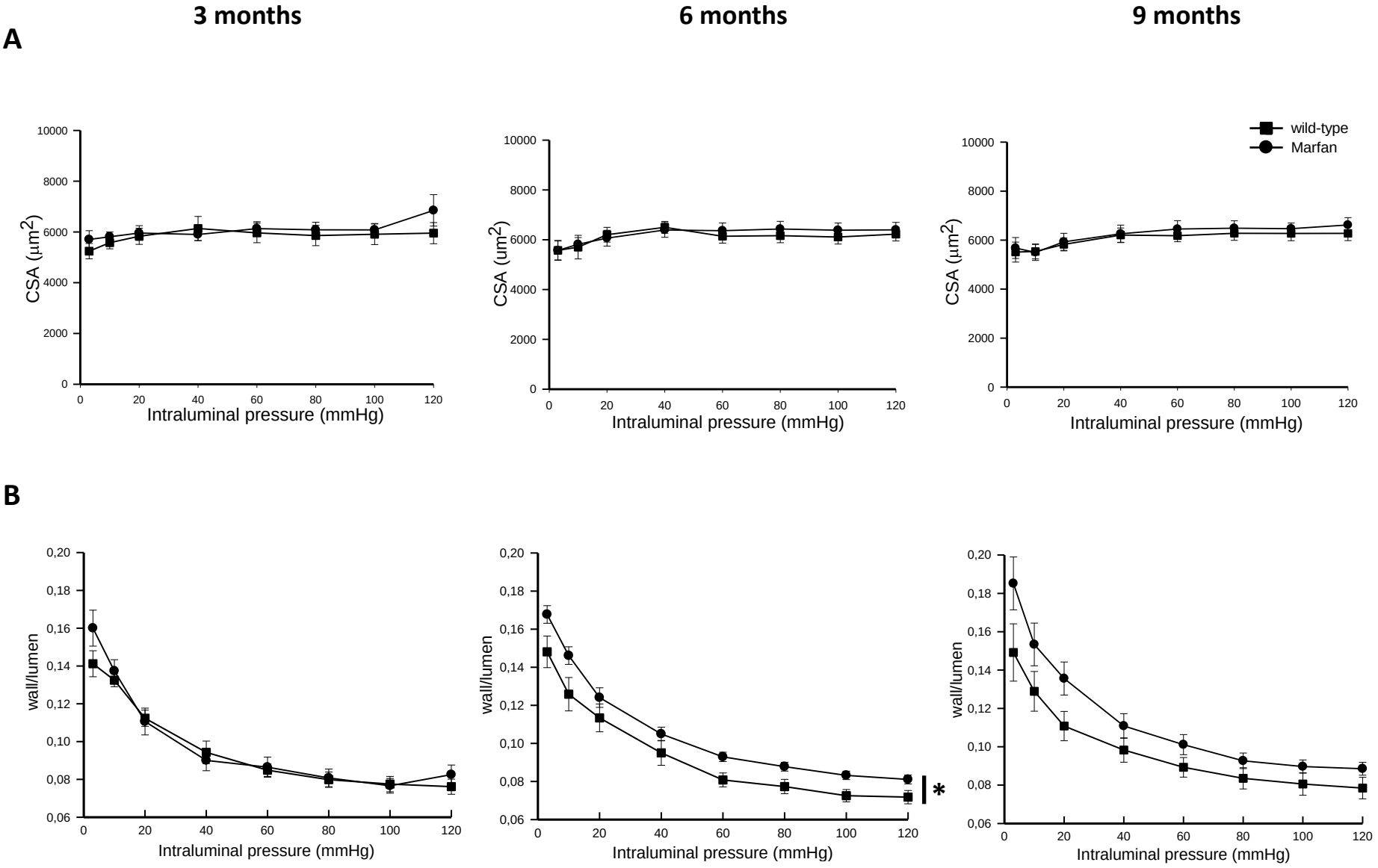
A
3 months
6 months
9 months
wild-type
Marfan
CSA (µm2)
CSA (um2)
Intraluminal pressure (mmHg)
B
wall/lumen
Intraluminal pressure (mmHg)
*

Fig. 2

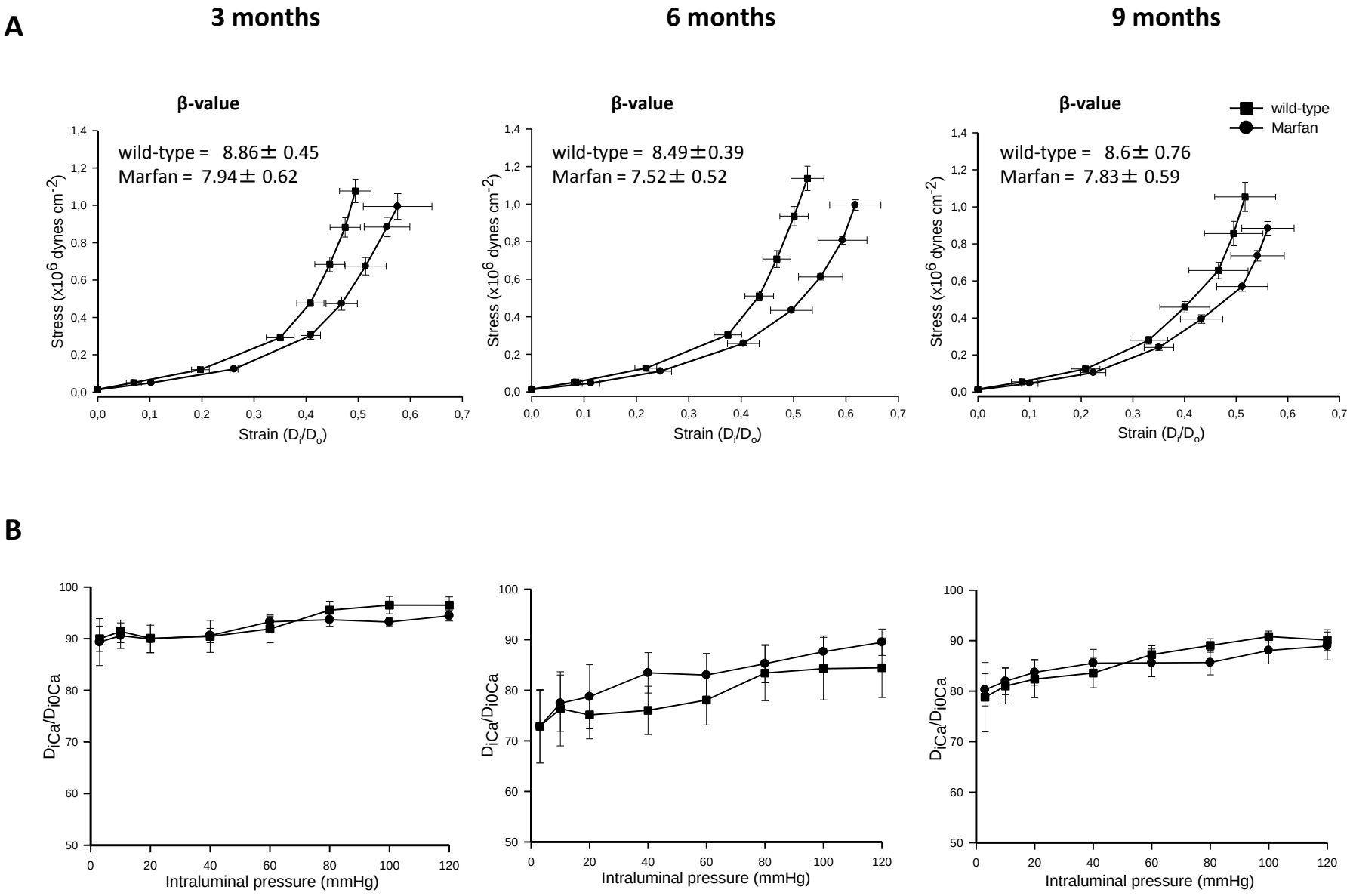
A
3 months
6 months
9 months
β-value
wild-type = 8.86± 0.45
Marfan = 7.94± 0.62
wild-type = 8.49±0.39
Marfan = 7.52± 0.52
wild-type = 8.6± 0.76
Marfan = 7.83± 0.59
wild-type
Marfan
Stress (x10^6 dynes cm^-2)
Strain (Di/Do)
B
DiCa/Di0Ca
Intraluminal pressure (mmHg)

Fig. 3

A

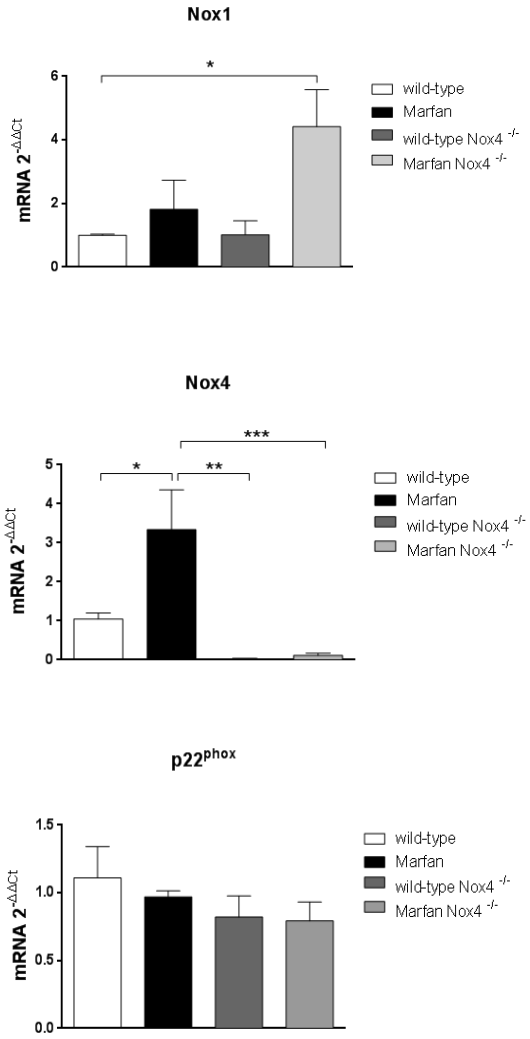
Nox1
mRNA 2^-ΔΔCt
wild-type
Marfan
wild-type Nox4 -/-
Marfan Nox4 -/-
Nox4
p22phox

B

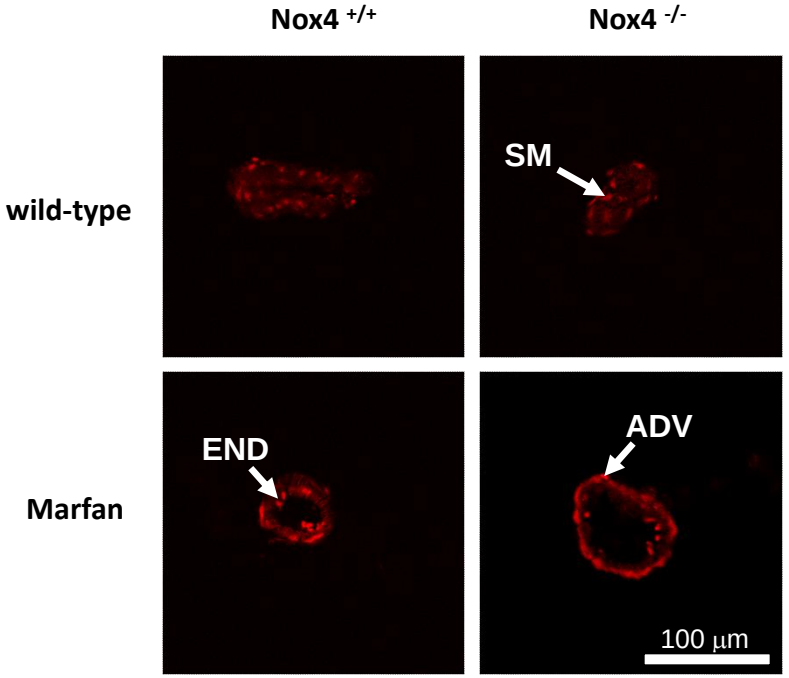
Nox4 +/+
Nox4 -/-
wild-type
Marfan
SM
END
ADV
100 µm

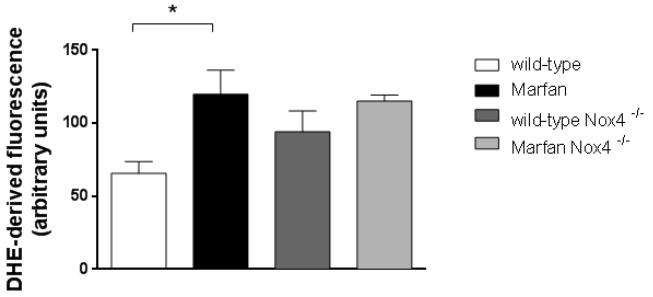
DHE-derived fluorescence (arbitrary units)
wild-type
Marfan
wild-type Nox4 -/-
Marfan Nox4 -/-

Fig. 4

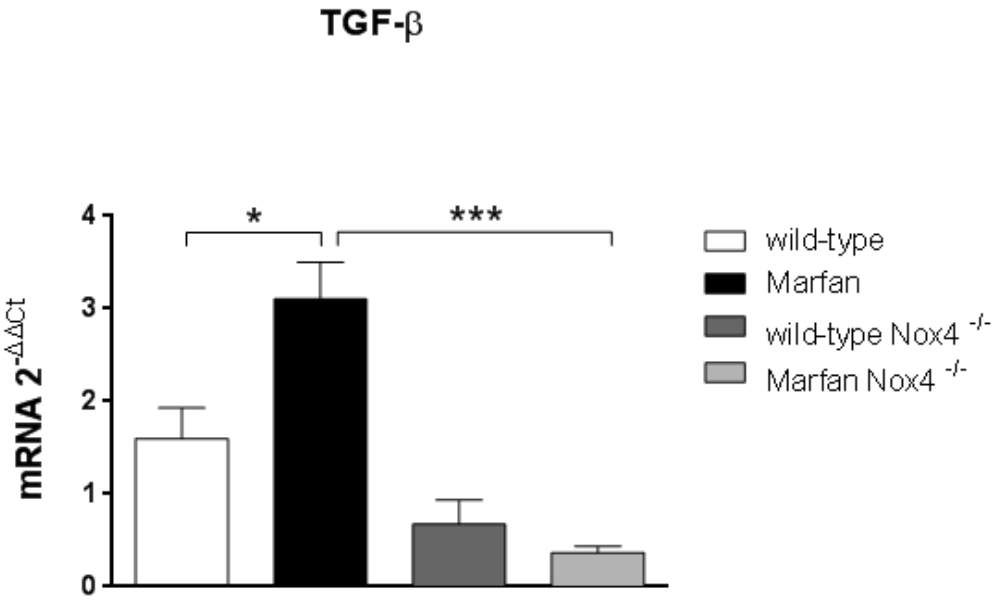
TGF-β
mRNA 2-ΔΔCt
0
1
2
3
4
*
***
wild-type
Marfan
wild-type Nox4 -/-
Marfan Nox4 -/-

Fig. 5

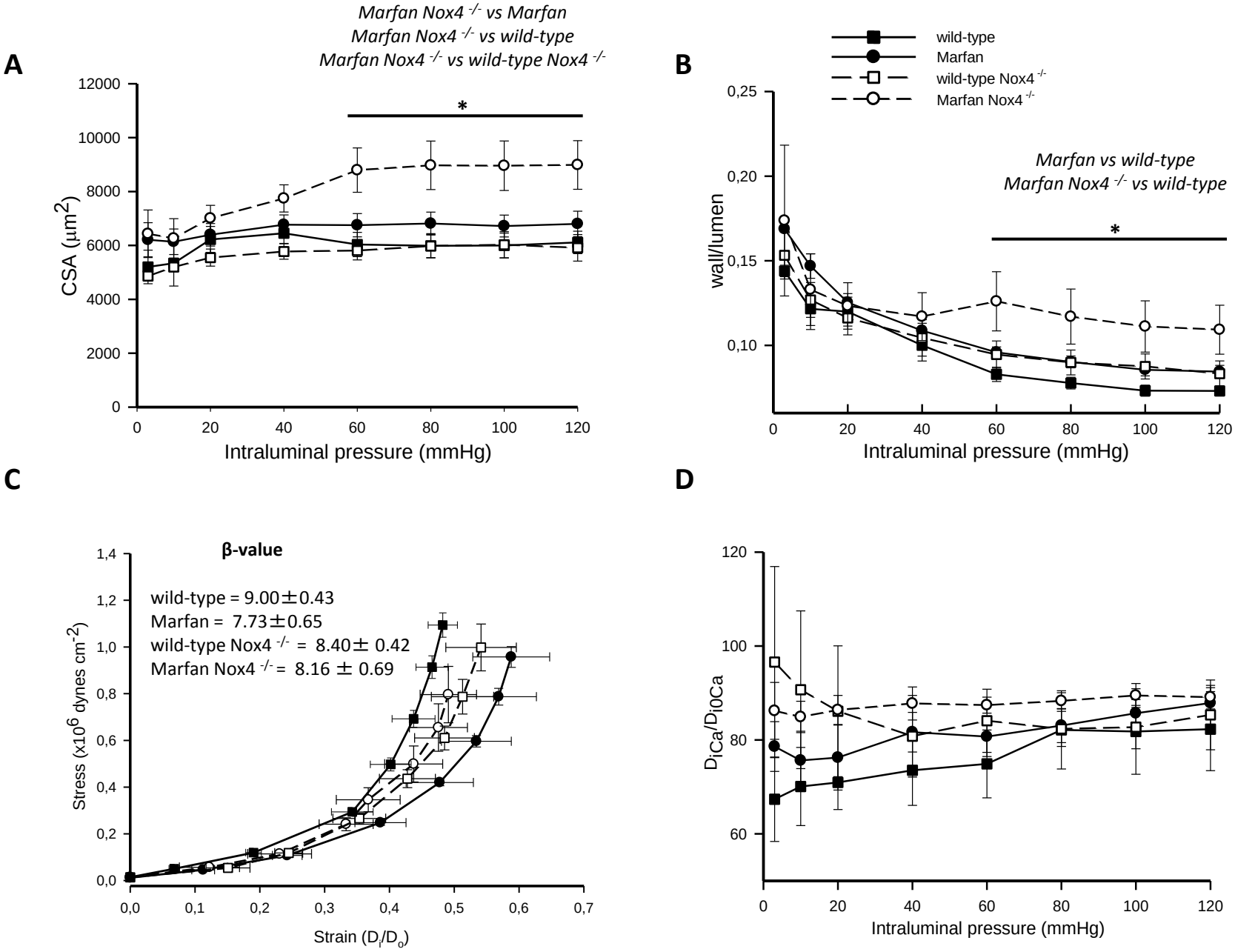
A
Marfan Nox4 -/- vs Marfan
Marfan Nox4 -/- vs wild-type
Marfan Nox4 -/- vs wild-type Nox4 -/-
CSA (µm2)
Intraluminal pressure (mmHg)
B
wild-type
Marfan
wild-type Nox4 -/-
Marfan Nox4 -/-
Marfan vs wild-type
Marfan Nox4 -/- vs wild-type
wall/lumen
Intraluminal pressure (mmHg)
C
β-value
wild-type = 9.00±0.43
Marfan = 7.73±0.65
wild-type Nox4 -/- = 8.40± 0.42
Marfan Nox4 -/- = 8.16 ± 0.69
Stress (x10^6 dynes cm^-2)
Strain (Di/Do)
D
DiCa/Di0Ca
Intraluminal pressure (mmHg)

Fig. 6

A

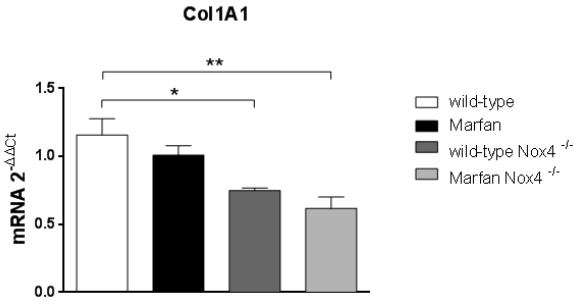
Col1A1
mRNA 2-ΔΔCt
1.5
1.0
0.5
0.0
**
*
wild-type
Marfan
wild-type Nox4 -/-
Marfan Nox4 -/-

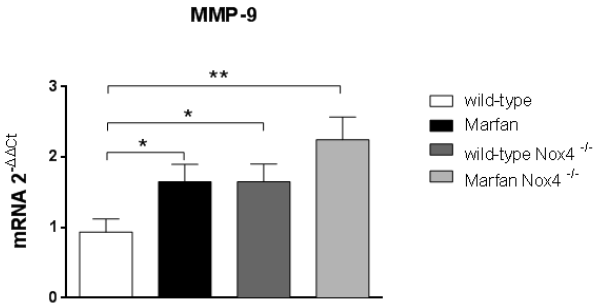
MMP-9
mRNA 2-ΔΔCt
3
2
1
0
**
*
*
wild-type
Marfan
wild-type Nox4 -/-
Marfan Nox4 -/-

B

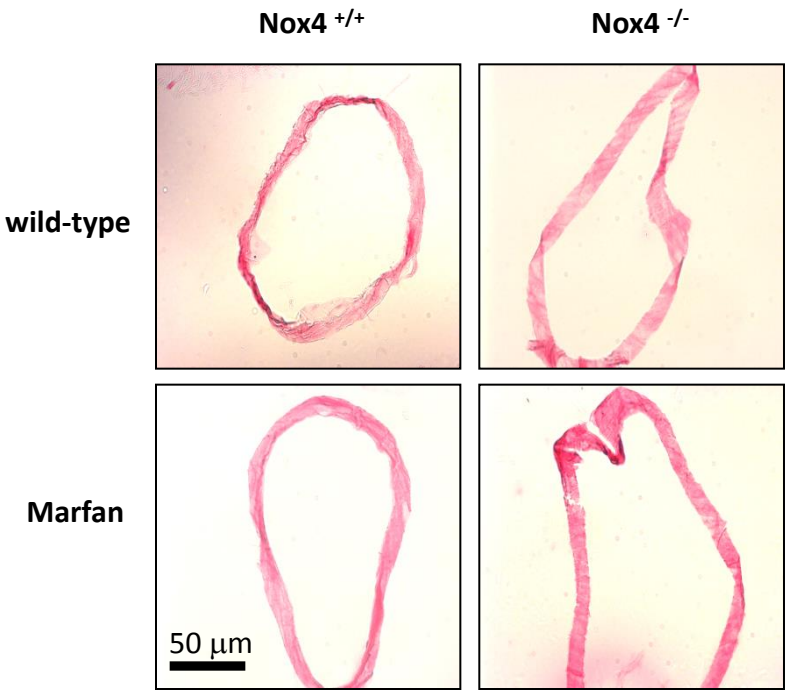
Nox4 +/+
Nox4 -/-
wild-type
Marfan
50 µm

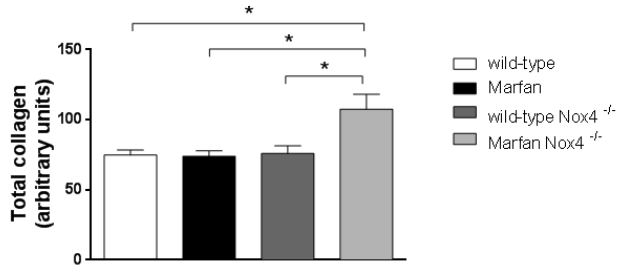
Total collagen (arbitrary units)
150
100
50
0
*
*
*
wild-type
Marfan
wild-type Nox4 -/-
Marfan Nox4 -/-

C

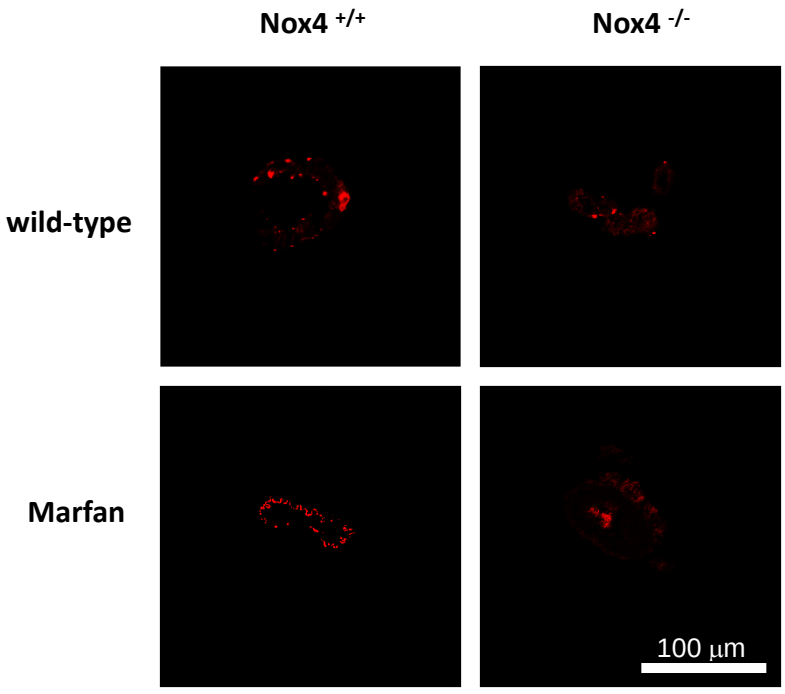
Nox4 +/+
Nox4 -/-
wild-type
Marfan
100 µm

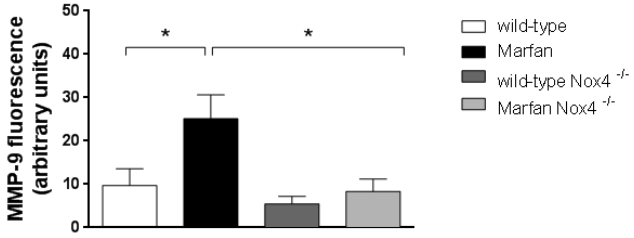
MMP-9 fluorescence (arbitrary units)
50
40
30
20
10
0
*
*
wild-type
Marfan
wild-type Nox4 -/-
Marfan Nox4 -/-